Journal of Nano- and Electronic Physics
Vol. **18** No 4, 04028(7pp) (2026)

Журнал нано- та електронної фізики
Том **18** № 4, 04028(7cc) (2026)

OPEN ACCESS

REGULAR ARTICLE

Tuning Structural and Optical Properties of Cu-Doped CdS Nanoparticles via Controlled Bandgap Engineering

Sikandar Kumar, J.P. Sharma* ✉

University Department of Physics, Dr. Shyama Prasad Mukharjee University, Ranchi-834001, India

(Received 05 May 2026; revised manuscript received 18 August 2026; published online 21 August 2026)

Cadmium sulfide (CdS) nanoparticles doped with copper ($Cd_{1-x}Cu_xS$) are synthesized using a chemical co-precipitation method to investigate the effect of Cu incorporation on the structural and optical properties, with particular emphasis on bandgap modulation. X-ray diffraction (XRD) analysis confirms the formation of a single-phase hexagonal CdS crystal structure without any detectable secondary phases, indicating the successful incorporation of Cu into the host lattice. A gradual reduction in crystallite size from 3.73 nm to 2.89 nm is observed with increasing Cu concentration. A slight decrease in the lattice parameters and unit cell volume further supports the substitution of Cd^{2+} ions by the relatively smaller Cu^{2+} ions.

Field Emission Scanning Electron Microscopy (FESEM) reveals nanostructured particles with moderate agglomeration, while Cu incorporation improves particle size uniformity. Energy Dispersive X-ray Analysis (EDAX) confirms the presence of Cd, S, and Cu elements and shows no evidence of impurity phases, verifying the successful incorporation of Cu into the CdS lattice. The optical properties are examined using UV-Visible spectroscopy, which shows a progressive blue shift in the absorption edge with increasing Cu content. The optical bandgap increases from 2.08 eV for pristine CdS to 2.15 eV and 2.16 eV for the Cu-doped compositions. This bandgap widening is attributed to the combined influence of quantum confinement arising from the reduced crystallite size and lattice distortion associated with Cu substitution. These findings demonstrate that Cu doping provides an effective approach for tuning the structural and optical properties of CdS nanoparticles, highlighting their potential for optoelectronic and photocatalytic applications.

Keywords: Cu-doped CdS nanoparticles, Bandgap engineering, Quantum confinement, Chemical co-precipitation, Optical properties, XRD, FESEM, EDAX, Photocatalysis.

DOI: 10.21272/jnep.18(4).04028 PACS numbers: 81.07.Wx, 78.67.Bf, 81.16.Be, 71.20.Nr

1. INTRODUCTION

II-VI group semiconductors are important materials in modern materials science. They possess versatile structural, electronic, and optical properties. These properties make them useful for many technological applications. They are widely used in photocatalysis and light-emitting diodes. They also find applications in sensors and solar cells [1]. They are also used in biomedical imaging technologies. Cadmium sulfide (CdS) is an important II-VI semiconductor material [2]. It has a direct band gap and strong absorption in the visible region. CdS also exhibits high photosensitivity. It is a widely studied *n*-type semiconductor. The band gap of CdS is about 2.42 eV at room temperature [3]. CdS is commonly used as a window material in heterojunction solar cells [4]. It is also applied in photodetectors and optoelectronic devices. CdS exists in cubic (zinc blende) and hexagonal (wurtzite) crystal structures [5]. These structures provide different optical and electronic properties. CdS nanoparticles can be synthesized using several techniques. Common methods include sol-gel, thermal evaporation, and chemical vapor deposition[6-8]. Hydrothermal and co-precipitation methods are also widely used [9, 10]. Among these, chemical co-precipitation is simple and cost-effective. It can be performed at room temperature. This method can produce relatively uniform nanoparticles. It also allows control over particle size and morphology. These factors strongly influence the quantum confinement effect. When the particle size approaches the Bohr exciton radius of CdS (~ 2.9 nm), quantum confinement occurs [11]. This effect modifies the electronic structure of the nanoparticles. As a result, the band gap becomes wider. The optical absorption edge shifts toward shorter wavelengths. This shift is commonly known as a blue shift. Nanocrystals also possess a high surface-to-volume ratio [12]. Surface states therefore play a significant role in their properties. These surface states strongly influence the optical emission behavior. Doping with transition metal ions is an effective way to modify CdS properties. It helps tailor the physical and optical characteristics of the material. Doping can alter the electronic band structure. It may also introduce localized energy states. These changes can enhance luminescence efficiency. They can also improve photoconductivity and magnetic behavior. Among the transition metals, copper (Cu^{2+}) has attracted considerable interest as a dopant because its ionic radius (0.57 Å) is comparable to that of Cd^{2+} (0.95 Å), enabling substitutional incorporation into the CdS lattice [13].

* Correspondence e-mail: sharmajp.rcr@gmail.com

Cite this article as: S. Kumar et al., *J. Nano- Electron. Phys.* 18 No 4, 04028 (2026) https://doi.org/10.21272/jnep.18(4).04028

Incorporation of Cu is reported to introduce acceptor levels within the band gap, which enhances optical absorption and can produce defect-related visible emissions, making Cu-doped CdS a promising material for optoelectronic and photovoltaic devices. This work reported the synthesis of $Cd_{1-x}Cu_xS$ (x = 0.01 and 0.03 nanoparticles at room temperature using the chemical co-precipitation method. The structural, morphological, and optical properties of the samples were systematically investigated using XRD, FESEM, EDAX and UV-Visible spectroscopy which explore the effect of Cu doping on the crystallite size, morphology, and band gap of CdS nanoparticles for optoelectronic applications.

2. MATERIALS AND METHOD

2.1 Materials

Cadmium acetate dihydrate ($Cd(CH_3COO)_2{\cdot}2H_2O$), copper chloride dihydrate ($CuCl_2{\cdot}2H_2O$), thiourea $CS(NH_2)_2$, and sodium sulphide (Na_2S) were used as precursor chemicals for the synthesis of CdS and Cu-doped CdS nanoparticles. All reagents were of analytical grade and were used without further purification. Distilled water was used as the solvent for preparing all aqueous solutions, while ethanol and distilled water were used for washing the synthesized precipitates.

2.2 Methodology

2.2.1 Synthesis of CdS Nanoparticles

CdS nanoparticles were synthesized via a chemical co-precipitation method. In this process, 2.66 g of cadmium acetate dihydrate ($Cd(CH_3COO)_2{\cdot}2H_2O$) was dissolved in 100 mL of distilled water under continuous magnetic stirring to obtain a 0.1 M cadmium precursor solution. The solution was stirred for approximately 20 minutes to ensure complete dissolution of the precursor. Subsequently, 1.52 g of thiourea, $CS(NH_2)_2$ was added gradually to the cadmium acetate solution under constant stirring to facilitate the formation of a homogeneous reaction mixture. After complete mixing, an aqueous solution containing 0.78 g of sodium sulphide (Na_2S) dissolved in distilled water was added dropwise into the reaction system (Fig. 1).

The introduction of sulphide ions initiated the co-precipitation reaction between cadmium and sulphide ions [14]. This reaction produced a yellow precipitate of CdS nanoparticles according to:

$$Cd^{2+} + S^{2-} \rightarrow CdS\downarrow$$

The reaction mixture was continuously stirred using a magnetic stirrer. Stirring was maintained for 2 hours at room temperature. This ensured complete precipitation and proper growth of the nanoparticles. The obtained precipitate was separated by centrifugation at 5000 rpm for 10 min, followed by repeated washing with distilled water and ethanol to remove residual ions and impurities. Finally, the purified precipitate was dried in a hot air oven at 70 °C for 6 h to obtain CdS nanopowder.

2.2.2 Synthesis of Cu-Doped CdS Nanoparticles

Cu-doped CdS nanoparticles with different copper concentrations (1 % and 3 %) were synthesized using the same chemical co-precipitation method employed for the preparation of pure CdS, with the incorporation of copper ions as dopant precursors [15]. In this process, 2.66 g of cadmium acetate dihydrate ($Cd(CH_3COO)_2{\cdot}2H_2O$) was dissolved in 100 mL of distilled water under continuous magnetic stirring to obtain a 0.1 M cadmium precursor solution. After complete dissolution, a calculated amount of copper chloride dihydrate ($CuCl_2{\cdot}2H_2O$) was added to the cadmium precursor solution to achieve the desired dopant concentration. For 1 mol % Cu doping, 0.017 g of $CuCl_2{\cdot}2H_2O$ was added, whereas for 3 mol % Cu doping, 0.051 g of $CuCl_2{\cdot}2H_2O$ was introduced into the reaction mixture. The resulting mixed Cd^{2+}/Cu^{2+} precursor solution was stirred for approximately 20 minutes to ensure homogeneous distribution of copper ions in the solution.

Following this, 1.52 g of thiourea $CS(NH_2)_2$ was gradually added to the mixed precursor solution under continuous stirring to form a homogeneous reaction medium. Subsequently, an aqueous solution of 0.78 g sodium sulphide (Na_2S) dissolved in distilled water was added dropwise into the reaction mixture. The introduction of sulphide ions initiated the co-precipitation reaction between cadmium, copper, and sulphide ions, leading to the formation of Cu-doped CdS nanoparticles according to the reaction:

$$Cd^{2+} + Cu^{2+} + S^{2-} \rightarrow Cu{:}\,CdS$$

During the reaction, a yellowish to orange precipitate was formed, indicating the successful incorporation of copper ions into the CdS lattice. The reaction mixture was continuously stirred using a magnetic stirrer. Stirring was maintained for 2 hours at room temperature. This ensured complete nucleation and growth of the doped nanoparticles.

The resulting precipitate was separated by centrifugation at 5000 rpm for 10 minutes. It was washed several times with distilled water and ethanol. This step removed residual impurities and unreacted precursors. The purified precipitate was then dried in a hot air oven. Drying was carried out at 70 °C for 6 hours. Finally, 1 % and 3 % Cu-doped CdS nanopowders were obtained.

2.3 Characterization Techniques

The prepared samples were used for further characterization studies. Structural, morphological, and optical properties were investigated. The crystalline structure was examined using X-ray diffraction (XRD). CuKα radiation with a wavelength of 1.5406 Å was used for the analysis.

The diffraction patterns were recorded in the 2θ range of 20°-80° at an accelerating voltage of 40 kV, a tube current of 20 mA, and a scanning rate of 0.02°/s. The average crystallite size of the nanoparticles was estimated using the Debye-Scherrer equation.

The surface morphology of the synthesized nanoparticles was examined using a Field Emission Scanning Electron Microscopy (FESEM) and Energy Dispersive X-ray Spectroscopy (EDAX). FESEM provided information on particle size, shape, and agglomeration, while EDAX confirmed the elemental composition and successful incorporation of copper into the CdS lattice.

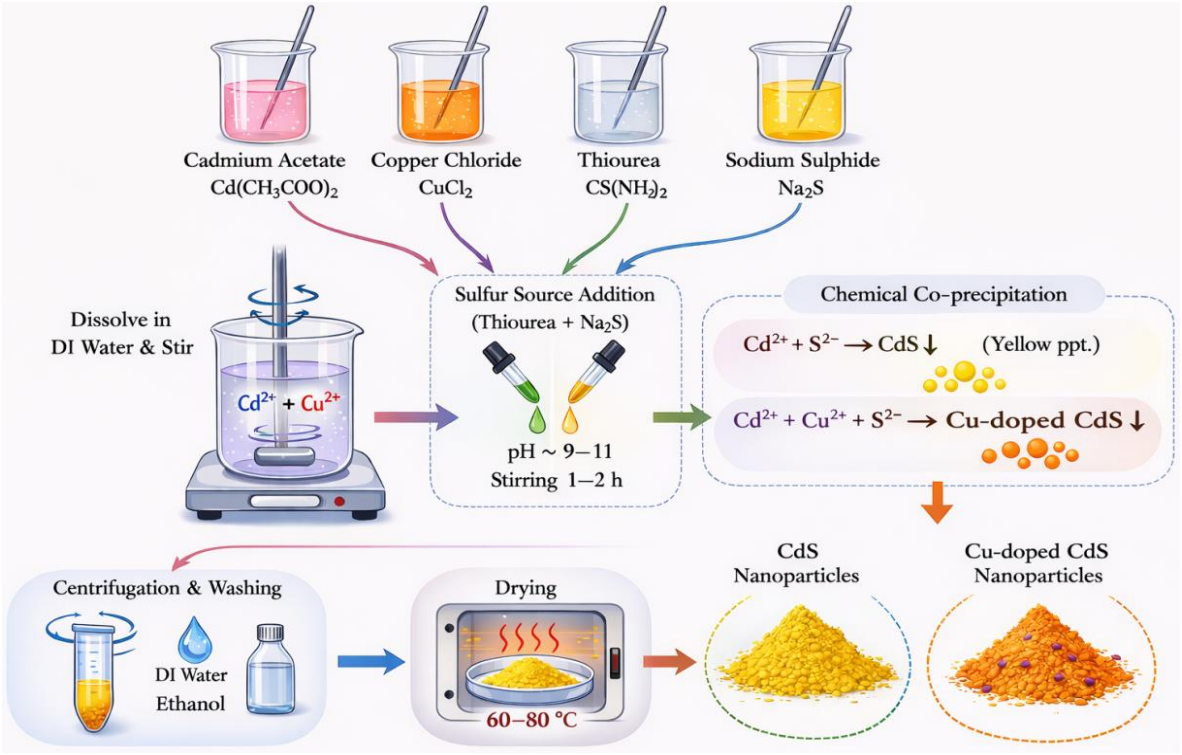

Fig. 1 – Schematic diagram of synthesis process

The optical absorption of pure CdS and Cu-doped CdS ($Cd_{1-x}Cu_xS$) nanoparticles were recorded using a UV-Visible spectrophotometer (Hitachi U3900, equipped with Varian Cary 50 software) in the wavelength range of 200-800 nm. The optical band gap values were calculated from Tauc's plots derived from the absorption spectra.

3. RESULTS AND DISCUSSION

3.1 Structural Properties

Fig. 2 shows the X-ray diffraction (XRD) patterns of $Cd_{1-x}Cu_xS$ nanoparticles with doping concentrations $x = 0$ %, 1 %, and 3 %. The prominent peaks at $2\theta = 26.74°$, 29.42°, 31.77°, 37.58°, 44.24°, and 52.27° correspond to the (002), (101), (102), (110), and (112) planes, respectively, and are consistent with the standard cubic CdS phase (JCPDS Card No. 10-0454) 5]. The peak broadening confirms the nanocrystalline nature of the samples. In both pure and Cu-doped CdS, the (002) reflection is the most intense, indicating a preferred orientation along this plane. No additional peaks corresponding to copper or secondary phases are observed, confirming the successful incorporation of Cu ions into the CdS lattice without impurity phase formation. A slight shift of the (002) peak toward higher angles is evident and becomes more pronounced with increasing Cu concentration, indicating lattice distortion. This distortion arises from the substitution of larger Cd^{2+} ions by smaller Cu^{2+} ions. The diffraction angle (2θ) and full width at half maximum (β) were extracted from the XRD data. Using these, the interplanar spacing (d), lattice parameter (a), average crystallite size (D), dislocation density (δ), and microstrain (ε) were calculated along the (002) plane. The corresponding values for $Cd_{1-x}Cu_xS$ ($x = 0$, 0.01, and 0.03) are summarized in Table 1.

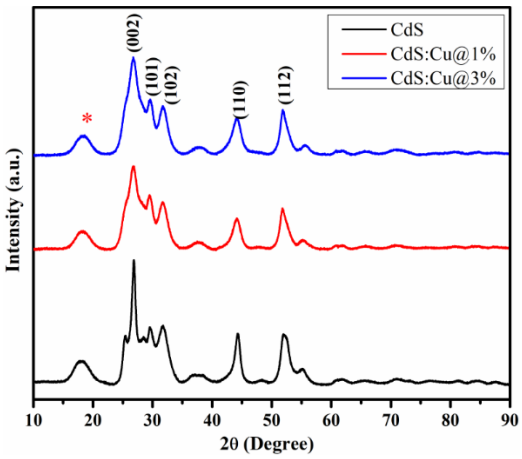

Fig. 2 – The X-ray diffraction (XRD) patterns of Cu:CdS at various concentrations

Crystallite Size (D)

The average crystallite size (D) was estimated from XRD peak broadening using the Debye-Scherrer equation [16]:

$$D = \frac{0.9\lambda}{\beta \cos\theta}$$

where $\lambda = 1.5406$ Å, β is the FWHM (in radians), and θ is the Bragg angle. The crystallite size decreases from ~ 3.73 nm for pure CdS to ~ 2.89 nm for CdS:Cu@3 %, indicating that Cu incorporation suppresses crystal growth. This reduction is attributed to substitution of smaller Cu^{2+} ions at Cd^{2+} sites, which introduces lattice strain, structural distortion, and defect centers. These defects hinder crystallite growth and increase grain boundaries, leading to smaller crystallites with higher defect density.

Table 1 – XRD parameters of CdS:Cu corresponding to (002) plane

Sample	2θ (°)	FWHM β (rad)	D (nm)	δ ($\times 10^{-2}$ nm^{-2})	ε ($\times 10^{-3}$)	a (nm)	c (nm)	V (nm^3)
CdS	26.74219	2.16147	3.7347	0.2140	2.2418	0.2513	0.4105	0.0224
CdS:Cu@1 %	26.74853	2.74748	2.9381	0.1325	2.8503	0.2512	0.4103	0.0224
CdS:Cu@3 %	26.76108	2.78918	2.8941	0.1285	2.8950	0.2511	0.4101	0.0223

The reduced size enhances surface-to-volume ratio, improving surface reactivity, optical response, and photocatalytic performance, confirming the strong influence of Cu doping on microstructural evolution.

Dislocation Density (δ)

Dislocation density (δ), representing the extent of lattice defects, was calculated using [17]:

$$\delta = \frac{1}{D^2}$$

The dislocation density increases slightly with Cu doping due to reduced crystallite size and dopant incorporation. Substitution of Cu^{2+} at Cd^{2+} sites introduces lattice strain and disturbs periodic atomic arrangement, generating defects such as dislocations and vacancies. Since δ is inversely proportional to crystallite size, its increase reflects enhanced defect density and lattice imperfections. These defects act as stress centers, influencing charge carrier mobility, optical absorption, and photocatalytic activity. The increase in δ confirms successful Cu incorporation and associated microstructural modifications.

Microstrain (ε)

Microstrain (ε), representing internal lattice distortion, was calculated from XRD broadening using [18]:

$$\varepsilon = \frac{\beta}{4\tan\theta}$$

The microstrain increases from 2.24×10^{-3} (pure CdS) to 2.89×10^{-3} (CdS:Cu@3 %), indicating increased internal strain due to Cu incorporation. Substitution of Cu^{2+} at Cd^{2+} sites introduces local distortions arising from differences in ionic size, electronic configuration, and bonding characteristics. These distortions generate strain fields and promote defect formation, including dislocations and point defects. The increase in ε is consistent with reduced crystallite size and higher dislocation density, confirming enhanced lattice disorder. Such strain affects electronic structure, band behavior, and charge carrier dynamics, thereby influencing optical and photocatalytic properties.

Lattice Parameters (a and c)

Lattice parameters were calculated assuming hexagonal CdS structure [19]. A slight decrease is observed with Cu doping: from a = 0.2513 nm and c = 0.4105 nm (pure CdS) to a = 0.2511 nm and c = 0.4101 nm (CdS:Cu@3 %). This contraction arises from substitution of smaller Cu^{2+} ions (0.73 Å) in place of larger Cd^{2+} ions (0.97 Å), leading to reduced interatomic spacing. The resulting lattice distortion agrees with increased microstrain and dislocation density, confirming substitutional incorporation of Cu without secondary phases. These structural changes influence electronic band structure, defect density, and carrier transport [20].

Unit Cell Volume (V)

The unit cell volume for hexagonal CdS was calculated using:

$$V = \frac{\sqrt{3}}{2}a^2c$$

The volume decreases slightly from ~ 0.0224 nm^3 (pure CdS) to ~ 0.0223 nm^3 (CdS:Cu@3 %), consistent with lattice contraction due to Cu substitution. The smaller ionic radius of Cu^{2+} reduces interatomic spacing, leading to a decrease in lattice parameters and unit cell volume. This observation aligns with XRD results, including reduced crystallite size, increased microstrain, and higher dislocation density. The contraction confirms successful Cu incorporation and dopant-induced structural modification, which in turn affects electronic structure, defect formation, and functional properties.

3.2 Optical Properties of CdS and Cu–Doped CdS Nanostructures

3.2.1 *UV*-Visible Absorption Analysis

The optical absorption spectra of pure CdS and Cu-doped CdS (CdS:Cu@1% and CdS:Cu@3 %) are presented in Fig. 3, recorded in the wavelength range of 200-800 nm. The study aims to examine the effect of Cu incorporation on the optical behavior of CdS nanostructures. All samples exhibit strong absorption in the ultraviolet region, which gradually decreases toward the visible region.

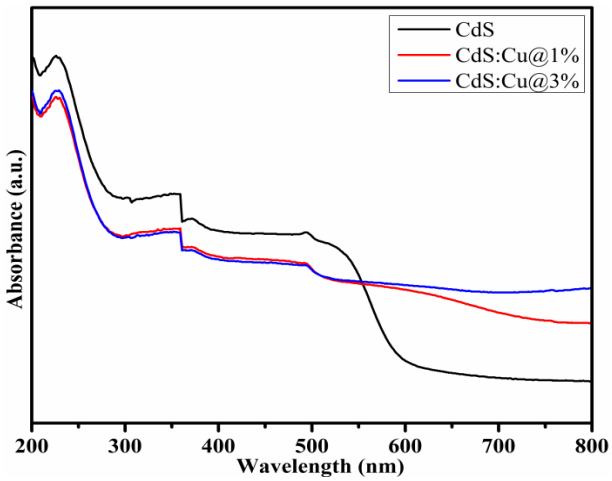

Fig. 3 – Optical absorption spectra

Pure CdS shows a sharp absorption edge around 590-600 nm, corresponding to its intrinsic band gap transition. Upon Cu doping, a slight blue shift in the

absorption edge is observed, indicating modification of the electronic structure due to dopant incorporation. This shift can be attributed to size reduction and dopant-induced changes in the band structure.

A slight decrease in absorption intensity is also observed for the doped samples compared to pure CdS. This behavior is associated with reduced crystallite size and increased lattice defects, which influence optical transitions. The incorporation of Cu ions introduces localized defect states and lattice distortions in the CdS structure, thereby altering the overall optical absorption characteristics.

3.2.2 Optical Band Gap Determination

The band gap value was obtained from the extrapolation of the Tauc plot [21]:

$$(\alpha h\nu)^2 = A(h\nu - E_g)$$

Here, α represents the absorption coefficient of the material. hv denotes the photon energy. A is a proportionality constant related to the transition probability. E_g corresponds to the optical band gap energy of the semiconductor.

The band gap values were determined from the T_{auc} plots. Plots of $(\alpha h\nu)^2$ versus photon energy ($h\nu$) were constructed. The linear region of the plot was extrapolated. The intersection with the energy axis gives the band gap value. The corresponding plots are shown in Fig. (4).

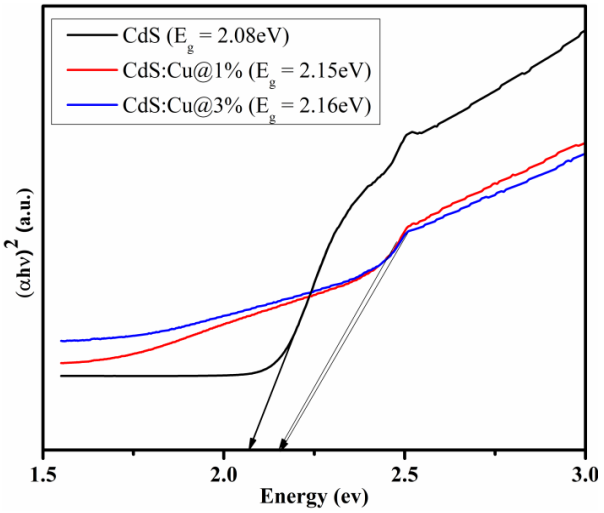

Fig. 4 – Tauc plots $(\alpha h\nu)^2$ versus ($h\nu$)

The optical band gap values increase gradually with Cu doping. Pure CdS shows a band gap of 2.08 eV. For CdS:Cu@1 %, the band gap increases to 2.15 eV. For CdS:Cu@3 %, it further increases to 2.16 eV. This trend indicates modification of the electronic structure. Cu incorporation slightly widens the band gap of CdS.

The results show that the band gap slightly increases with Cu concentration. This behavior can be explained by the quantum confinement effect. XRD results show a reduction in crystallite size. Smaller particles cause stronger confinement of charge carriers. This confinement leads to an increase in band gap energy. The incorporation of Cu ions introduces defect states in the CdS lattice.It also modifies the electronic band structure of the material. These changes contribute to the observed shift in band gap. The slight band gap widening indicates the effect of Cu doping. Thus, Cu incorporation alters the electronic properties of CdS nanostructures.

The combined UV-Vis and Tauc plot analysis confirms that Cu doping affects the optical properties of CdS nanoparticles. A blue shift of the absorption edge and increased band gap were observed. These changes indicate modification of the crystal and electronic structures by Cu ions. The results are consistent with XRD findings, including reduced crystallite size, increased micro strain, and higher dislocation density.

These modifications in optical properties are beneficial for photo catalysis, optoelectronics, and photodetectors. They can improve light absorption in the material. They also enhance charge carrier dynamics, boosting device performance.

3.3 Elemental and Morphological Studies

3.3.1 Morphological Analysis

The surface morphology of pure and Cu-doped CdS was examined using FESEM. Micrographs for pure CdS, CdS:Cu@1 %, and CdS:Cu@3 % are shown in Fig. 5(a-c). These images reveal the shape, size, and distribution of the nanoparticles. The FESEM image of pure CdS (Fig. 5a) shows densely packed nanostructured particles. The particles are irregular in shape and exhibit slight agglomeration. Such agglomeration is typical for semiconductor nanoparticles due to high surface energy. The microstructure reveals granular and clustered nanocrystals. This indicates a high nucleation rate during the synthesis process. For the CdS:Cu@1 % sample (Fig. 5b), the morphology shows more compact and aggregated nanostructures. The particles exhibit a slightly rougher surface and increased clustering compared to pure CdS. These changes are attributed to the incorporation of Cu ions into the CdS lattice. Cu doping influences the crystal growth mechanism. It also affects particle aggregation and nucleation behavior during synthesis. For the CdS:Cu@3 % sample (Fig. 5c), the FESEM image shows finer particles with a more uniform distribution. Higher Cu concentration appears to suppress excessive grain growth. This results in smaller and more densely distributed nanoparticles. These observations are consistent with XRD results showing reduced crystallite size. FESEM analysis confirms that Cu doping influences surface morphology and particle size distribution of CdS nanostructures. The similar results also found by Shaban, Mohamed et al. [22].

3.3.2 Elemental Analysis (EDAX)

The elemental composition of the samples was analyzed using EDAX, with spectra shown in Fig. 5(d-f). The EDAX spectrum of pure CdS (Fig. 5d) displays prominent peaks for cadmium (Cd) and sulfur (S). This confirms the formation of CdS nanoparticles. No additional peaks are observed, indicating high purity of the synthesized material. For the Cu-doped samples (Fig. 5e and 5f), EDAX shows peaks for Cd and S, as well as additional peaks for Cu. The presence of Cu peaks confirms successful incorporation of Cu ions into the CdS lattice. The intensity of the Cu peaks increases slightly with higher dopant concentration. This trend indicates controlled and effective doping of Cu in the CdS nanostructures.

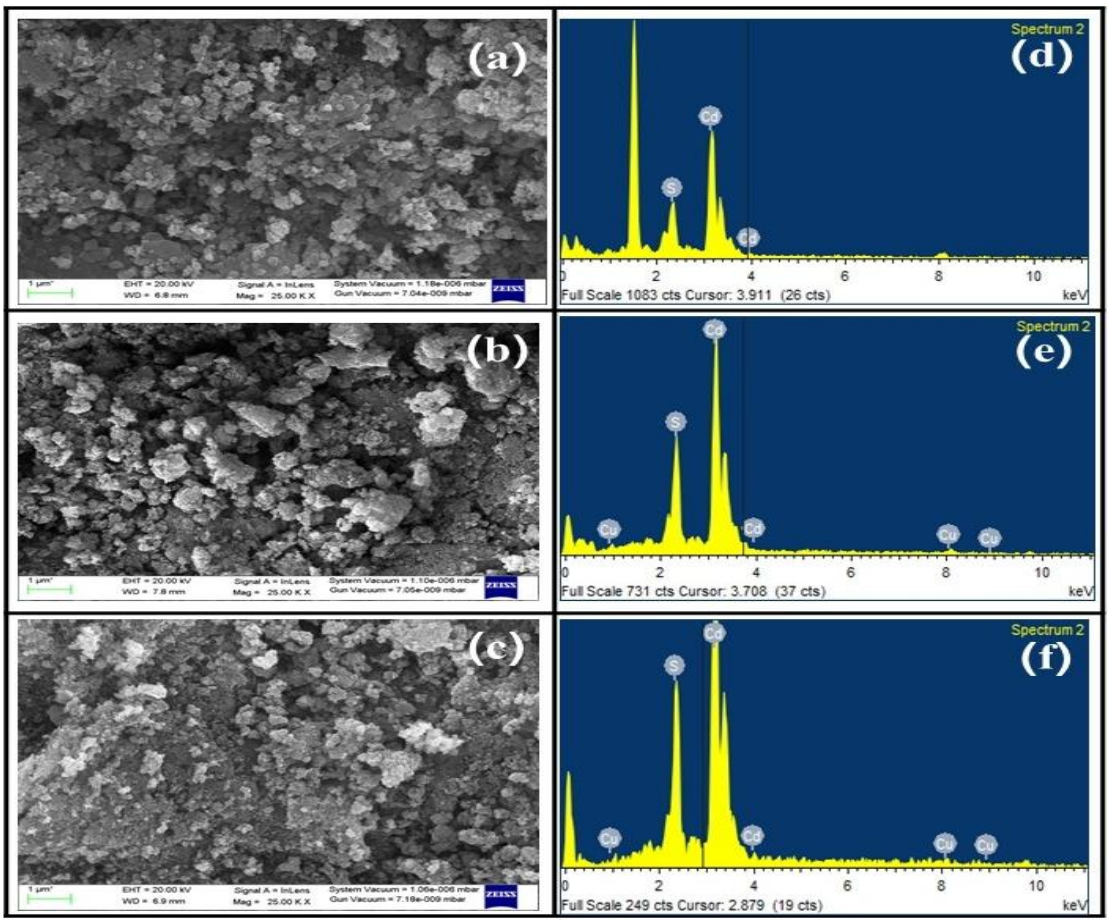

Fig. 5 – (a-c) FESEM micrographs and (d-f) EDAX spectra

The EDAX spectra show no significant impurity peaks, indicating high chemical purity of the CdS:Cu nanostructures. Similar work also has been reported by Nazari Setayesh, and Tiwary K.P., et al. [23, 24]. Combined FESEM and EDAX analyses confirm the formation of nanostructured CdS. They also verify successful incorporation of Cu ions and Cu doping modifies the surface morphology of the nanoparticles.

4. CONCLUSION

$Cd_{1-x}Cu_xS$ nanoparticles were successfully synthesized *via* chemical co-precipitation, exhibiting a hexagonal CdS structure without any detectable impurity phases, confirming effective Cu^{2+} incorporation into the lattice. XRD analysis revealed a systematic reduction in crystallite size along with peak shifts, indicating lattice contraction induced by substitution of Cd^{2+} with smaller Cu^{2+} ions. The increase in microstrain and dislocation density further suggests enhanced structural disorder upon doping. FESEM observations supported the XRD results, showing reduced particle size and improved uniformity with increasing Cu content, reflecting the influence of Cu on nucleation and growth kinetics. EDAX analysis confirmed the elemental composition and high chemical purity of the samples. Optical studies demonstrated a slight band gap widening with Cu incorporation, primarily attributed to quantum confinement effects and dopant-induced modifications in the electronic structure. Overall, Cu doping effectively tailors both the structural and optical properties of CdS nanoparticles, making $Cd_{1-x}Cu_xS$ a promising candidate for optoelectronic and energy-related applications.

DATA AVAILABILITY STATEMENT

The data sets generated and thereafter analyzed would be available from the corresponding author upon reasonable request.

CONFLICT OF INTEREST

The authors declare no competing interests.

FUNDING

This research work is not funded by any agency.

AUTHORSHIP CONTRIBUTION STATEMENT

Sikandar Kumar: Writing – review & editing, Writing – original draft, Methodology, Investigation, Formal analysis, Supervision, Conceptualization, Project administration, Funding acquisition. **J.P. Sharma:** Writing – review & editing, Supervision, Conceptualization, Project administration. Formal analysis.

REFERENCES

1. Maria C. Tamargo, *II-VI Semiconductor Materials and their Applications* Vol. **12** (CRC Press: 2002).
2. Ravi V. Ingle, et al., *Mater. Sci. Eng.: B* **294**, 116487 (2023) https://doi.org/10.1016/j.mseb.2023.116487.
3. K. Senthil, D. Mangalaraj, Sa K. Narayandass, *Appl. Surface Sci.* **169**, 476 (2001) https://doi.org/10.1016/S0169-4332(00)00732-7.
4. Taoufik Chargui, et al., *Opt. Mater.* **140**, 113849 (2023) https://doi.org/10.1016/j.optmat.2023.113849.
5. Jianbin Mao, Weiming Xu, Soonmin Seo, *J. Mater. Chem. A* **12** No 35, 23218 (2024) https://doi.org/10.1039/d4ta03496a.
6. Rakesh K. Sonker, et al., *Mater. Chem. Phys.* **239**, 121975 (2020) https://doi.org/10.1016/j.matchemphys.2019.121975.
7. Nafiseh Memarian, et al., *Materials* **10** No 7, 773 (2017) https://doi.org/10.3390/ma10070773.
8. Hiroshi Uda, et al., *Sol. Energy Mater. Sol. C.* **75** No 1-2, 219 (2003) https://doi.org/10.1016/S0927-0248(02)00163-0.
9. Yuexiang Li, et al., *J. Phys. Chem. C* **113** No 21, 9352 (2009) https://doi.org/10.1021/jp901505j.
10. B. Srinivasa Rao, et al., *Chalcogenide Lett.* **8** No 3, 177 (2011) https://chalcogen.ro/177_Srinivasa-Rao.pdf.
11. M. Thambidurai, et al., *J. Mater. Sci.* **45** No 12, 3254 (2010) https://doi.org/10.1007/s10853-010-4333-7.
12. Rohit Singh, Bonamali Pal, *Mater. Res. Bull.* **48** No 4, 1403 (2013) https://doi.org/10.1016/j.materresbull.2012.12.027.
13. Kadhim R. Gbashi, et al., *Appl. Phys. A* **126** No 8, 628 (2020) https://doi.org/10.1007/s00339-020-03801-1.
14. Ankit Goyal, et al., *J. Nano- Electron. Phys.* **3** No 1, 254 (2011) https://jnep.sumdu.edu.ua/en/component/content/full_article/168.
15. L.Q. Qian, et al., *J. Alloy. Compd.* **477** No 1-2, 888 (2009) https://doi.org/10.1016/j.jallcom.2008.11.007.
16. Prashanta Patra, et al., *Mater. Today: Proc.* (2023) https://doi.org/10.1016/j.matpr.2023.07.018.
17. Prashanta Patra, et al., *J. Crystal Growth* **583**, 126542 (2022) https://doi.org/10.1016/j.jcrysgro.2022.126542.
18. L.H. Qian, et al., *Acta Materialia* **50** No 13, 3425 (2002) https://doi.org/10.1016/S1359-6454(02)00155-6.
19. Fatma Göde, *Optik* **197**, 163217 (2019) https://doi.org/10.1016/j.ijleo.2019.163217.
20. A. Mukherjee, et al., *Mater. Chem. Phys.* **184**, 101 (2016) https://doi.org/10.1016/j.matchemphys.2016.09.030.
21. Kang'ethe Michael Ngahu, *Optical and electrical analysis of $Cd_{1-x}Fe_xS/CuS$ pn junction for solar cell application*. Diss. School of Pure and Applied Sciences of Kenyatta University (2016).
22. Mohamed Shaban, Mona Mustafa, A.M. El Sayed, *Mater. Sci. Semicond. Proc.* **56**, 329 (2016) https://doi.org/10.1016/j.mssp.2016.09.006.
23. Atefeh Nazari Setayesh, Sahar Moradi, Hasan Sedghi, *J. Nanopart. Res.* **25** No 1, 4 (2023) https://doi.org/10.1007/s11051-022-05653-7.
24. K.P. Tiwary, et al., *Mater. Today: Proc.* **18**, 1380 (2019) https://doi.org/10.1016/j.matpr.2019.06.604.

Налаштування структурних та оптичних властивостей наночастинок CdS, легованих міддю, за допомогою інженерії контрольованої забороненої зони

Sikandar Kumar, J.P. Sharma

University Department of Physics, Dr. Shyama Prasad Mukharjee University, Ranchi-834001, India

Наночастинки сульфіду кадмію (CdS), леговані міддю ($Cd_{1-x}Cu_xS$), синтезовані методом хімічного спільного осадження для дослідження впливу включення Cu на структурні та оптичні властивості, з особливим акцентом на модуляцію ширини забороненої зони. Рентгенівська дифракція (XRD) підтверджує формування однофазної гексагональної кристалічної структури CdS без будь-яких виявлених вторинних фаз, що свідчить про успішне включення Cu в кристалічну решітку. Спостерігається поступове зменшення розміру кристалітів від 3,73 нм до 2,89 нм зі збільшенням концентрації Cu. Незначне зменшення параметрів решітки та об'єму елементарної комірки додатково підтверджує заміщення іонів Cd^{2+} відносно меншими іонами Cu^{2+}.

Польова емісійна скануюча електронна мікроскопія (FESEM) виявляє наноструктуровані частинки з помірною агломерацією, тоді як включення Cu покращує однорідність розміру частинок. Енергетико-дисперсійний рентгенівський аналіз (EDAX) підтверджує наявність елементів Cd, S та Cu і не показує ознак домішкових фаз, що підтверджує успішне включення Cu в решітку CdS. Оптичні властивості досліджуються за допомогою УФ-видимої спектроскопії, яка показує прогресуючий зсув краю поглинання до синього кольору зі збільшенням вмісту Cu. Оптична заборонена зона збільшується з 2,08 еВ для чистого CdS до 2,15 еВ та 2,16 еВ для композицій, легованих Cu. Це розширення забороненої зони пояснюється комбінованим впливом квантового обмеження, що виникає внаслідок зменшення розміру кристалітів та спотворення решітки, пов'язаного із заміщенням Cu. Ці результати демонструють, що легування Cu забезпечує ефективний підхід до налаштування структурних та оптичних властивостей наночастинок CdS, підкреслюючи їхній потенціал для оптоелектронних та фотокаталітичних застосувань.

Ключові слова: Наночастинки CdS, леговані Cu, Інженерія забороненої зони, Квантове обмеження, Хімічне співосадження, Оптичні властивості, Рентгенівська дифракція (XRD), Електромагнітна скануюча мікроскопія (FESEM), Електромагнітна декомпозиція (EDAX), Фотокаталіз.